scientific reports

Check for updates

OPEN

Development of an efficient NUPR1 inhibitor with anticancer activity

Xi Liu[1,14], Ana Jimenez-Alesanco[2,14], Zexian Li[3], Bruno Rizzuti[2,4], José L. Neira[2,5], Matías Estaras[1], Ling Peng[6], Eduardo Chuluyan[7,8], Juan Garona[9,10], Florencia Gottardo[9,10], Adrián Velazquez-Campoy[2,11,12,13], Yi Xia[3], Olga Abian[2,11,12,13], Patricia Santofimia-Castaño[1✉] & Juan Iovanna[1,9,10✉]

Pancreatic cancer is highly lethal and has limited treatment options available. Our team had previously developed ZZW-115, a promising drug candidate that targets the nuclear protein 1 (NUPR1), which is involved in pancreatic cancer development and progression. However, clinical translation of ZZW-115 was hindered due to potential cardiotoxicity caused by its interaction with the human Ether-à-go-go-Related Gene (hERG) potassium channel. To address this, we have performed a high-throughput screening of 10,000 compounds from the HitFinder Chemical Library, and identified AJO14 as a lead compound that binds to NUPR1, without having favorable affinity towards hERG. AJO14 induced cell death through apoptosis, necroptosis, and parthanatos (induced by the poly-ADP ribose polymerase (PARP) overactivation), driven by mitochondrial catastrophe and decreased ATP production. This process seemed to be mediated by the hyperPARylation (an excessive modification of proteins by PARP, leading to cellular dysfunction), as it could be reversed by Olaparib, a PARP inhibitor. In xenografted mice, AJO14 demonstrated a dose-dependent tumor reduction activity. Furthermore, we attempted to improve the anti-cancer properties of AJO14 by molecular modification of the lead compound. Among the 51 candidates obtained and tested, 8 compounds exhibited a significant increase in efficacy and have been retained for further studies, especially LZX-2-73. These AJO14-derived compounds offer potent NUPR1 inhibition for pancreatic cancer treatment, without cardiotoxicity concerns.

Abbreviations

hERG	Human Ether-à-go-go-Related Gene
PARP	Poly-ADP ribose polymerase
PDAC	Pancreatic ductal adenocarcinoma
TSA	Thermal-shift assay
LB	Luria–Bertani broth
DMSO	Dimethyl sulfoxide
ANS	Extrinsic fluorescent probe 8-anilino-1-naphthalene sulfonic acid

[1]Centre de Recherche en Cancérologie de Marseille (CRCM), INSERM U1068, CNRS UMR7258, Aix Marseille Université and Institut Paoli Calmettes, Parc Scientifique etTechnologique de Luminy, Equipe labéliséeLigue Nationale contre le cancer, 163 Avenue de Luminy, 13288 Marseille, France. [2]Instituto de Biocomputación y Física de Sistemas Complejos (BIFI), 50018 Zaragoza, Spain. [3]Chongqing Key Lab oratory of Natural Product Synthesis and Drug Research, School ofPharmaceutical Sciences, Chongqing University, No.55 Daxuecheng South Road, Chongqing 401331, People's Republic of China. [4]CNR NANOTEC, SS Rende (CS), Department of Physics, University of Calabria, Via P.Bucci, Cubo 31 C, 87036 Rende, Italy. [5]IDIBE, Universidad Miguel Hernández, Edificio Torregaitán, Avda. del Ferrocarril s/n, 03202 Elche, Alicante, Spain. [6]Aix Marseille Université, CNRS, Centre Interdisciplinaire de Nanoscience de Marseille, UMR7325, Parc Scientifique et Technologique de Luminy, Equipe labélisée Ligue Nationale contre le cancer, 163 Avenue de Luminy, 13288 Marseille, France. [7]Center for Pharmacological and Botanical Studies, Faculty of Medicine, National Council for Scientific and Technical Research, Buenos Aires University, C1121ABG Buenos Aires, Argentina. [8]Department of Microbiology, Parasitology and Immunology, Faculty of Medicine, Buenos Aires University, C1121ABG Buenos Aires, Argentina. [9]Hospital de Alta Complejidad El Cruce, Florencio Varela, Buenos Aires, Argentina. [10]University Arturo Jauretche, Florencio Varela, Buenos Aires, Argentina. [11]Aragon Institute for Health Research (IIS Aragon), Zaragoza, Spain. [12]Centro de Investigación Biomédica en Red en el Área Temática de Enfe rmedadesHepáticas y Digestivas (CIBERehd), Madrid, Spain. [13]Departamento de Bioquímica y Biología Molecular y Celular, Universidad de Zaragoza, Zaragoza, Spain. [14]These authors contributed equally: Xi Liu and Ana Jimenez-Alesanco. ✉email: patricia.santofimia@inserm.fr; juan.iovanna@inserm.fr

IDP	Intrinsically disordered protein
ITC	Isothermal titration calorimetry
HSQC	2D 1H-15N heteronuclear single-quantum coherence
DMEM	Dulbecco's modified Eagle's medium
LDH	Lactate dehydrogenase
HRP	Horseradish peroxidase
DAB	Diaminobenzidine
OCR	Oxygen consumption rate
OXPHOS	Mitochondrial oxidative phosphorylation system

Pancreatic cancer has the highest mortality rate among all cancers, with a 5-year relative survival rate of only 8%, being the fourth leading cause of cancer death in the world[1]. Therefore, it remains a significant concern in the global cancer load[2]. According to Global Cancer Statistics 2020, 495,773 people worldwide were newly diagnosed with pancreatic cancer, and 466,003 people died from this disease[3]. More than 90% of diagnosed pancreatic cancer cases correspond to pancreatic ductal adenocarcinoma (PDAC). PDAC is normally treated with surgery, chemotherapy, and radiation therapy, but it is rarely curable. Less than 20% of PDAC patients can undergo surgical removal of tumors due to late-stage detection or metastasis to other organs, such as liver, lymph nodes, lungs, peritoneum and bones[4,5]. This makes chemotherapy the primary treatment option for PDAC. The current first-line chemotherapy options include treatment with FOLFIRINOX (5-fluorouracil, oxaliplatin, and irinotecan) and gemcitabine alone or in combination with nab-paclitaxel[6,7]. However, the overall survival rate of PDAC patients remains poor, and they are prone to relapse. Therefore, we urgently need to discover new therapeutic targets and develop new drugs for this highly fatal disease.

The nuclear protein 1 (NUPR1) is an intrinsically disordered protein (IDP) that plays a crucial role in cellular stress[8–10]. Furthermore, NUPR1 is specifically overexpressed in PDAC compared to its negligible expression in normal tissues, highlighting that this protein is a potential therapeutic target in PDAC[11]. Numerous studies have demonstrated that NUPR1 is involved in various PDAC-related processes, including its occurrence, development and metastasis[12]. However, finding inhibitors for NUPR1 poses significant challenges to traditional structure-based drug design, due to its disordered structure and multiple functions[10,13–16]. To overcome these challenges, we have previously employed a mid-throughput screening procedure based on the thermal-shift assay (TSA) to repurpose the antipsychotic drug trifluoperazine as a NUPR1 inhibitor[17]. This work was followed by computer modeling and chemical synthesis to improve the lead compound identified[18,19], and a range of biochemical, biophysical, and biological techniques to test the efficacy of the derivatives obtained. These studies led to the development of ZZW-115, a potent NUPR1 inhibitor. This compound was capable of effectively blocking NUPR1, resulting in the suppression of tumor cell growth both in vivo and in vitro[18]. However, as a trifluoperazine analogue, ZZW-115 has the potential to bind to the potassium ion channel encoded by the human Ether-à-go-go-Related Gene (hERG), leading to an inhibitory effect on this channel[20]. Indeed, drug-induced blockade of hERG remains a major impediment in delivering safe drugs to the market. As a result, there is a risk of cardiotoxicity associated with its use[21,22]. Specifically, binding to the hERG channel poses a risk of blocking the fast-delayed rectifier current I_{Kr} of the heart, thus delaying repolarization of the cardiac action potential and lengthening the QT interval and, therefore, putting the patients at increased risk of experiencing *torsades de pointes* and even sudden death[23,24]. For this reason, we need to find and develop new NUPR1 inhibitors without cardiotoxicity effects.

To this aim, in this work, we initially employed a screening method based on TSA with 10,000 compounds (HitFinder Chemical Library, from Maybridge Company), and identified 15 hit compounds (the so-called AJO series) with significant binding affinity to NUPR1. We evaluated 14 of the 15 hits (with the exception of AJO5, which was not further evaluated due to its low solubility) for their anticancer effect, by using a cell-based in vitro assay. As a result, we identified a lead compound, AJO14, which exhibited the most promising IC_{50}, with minimal binding to the hERG channel even at high concentrations. Notably, AJO14 primarily induced cell death through apoptosis, necroptosis, and parthanatos, accompanied by mitochondrial metabolism failure resulting in a substantial decrease in ATP production. This process seems to be mediated by hyperPARylation (an excessive modification of proteins leading to cellular dysfunction), driven by PARP, as it could be reversed by Olaparib, a PARP inhibitor. Finally, we attempted to improve the anti-cancer properties of AJO14 by molecular modification of the lead compound. Among the 51 new developed derivatives, 8 of them exhibited a significant increase in efficacy and have been retained for further studies, especially LZX-2-73. Taken together, our results indicate that AJO14-derived compounds are new potent NUPR1 inhibitors for treating PDAC without risk of cardiotoxicity.

Results
Identification of compounds interacting with NUPR1
A collection of 10,000 compounds (HitFinder Chemical Library, from Maybridge Company) was screened in vitro, according to a procedure based on thermal denaturation of ligand-driven partially-folded NUPR1 protein regions, applying the TSA protocol. From this screening, 15 compounds were selected and identified (from now, on named AJO1 to AJO15), as those capable of producing different temperature denaturation profiles in NUPR1 (Fig. 1A), when compared to the control (unliganded NUPR1) (Fig. 1B).

Interaction between NUPR1 and the AJO compounds
Experimental molecular screening always requires target engagement confirmation. Thus, after identifying compounds through the in vitro experimental screening by ligand-induced stabilization of NUPR1, it was necessary to verify their interaction with NUPR1, as well as to measure their binding affinity. There is no direct correlation between the extent of the protein structural stabilization, or the magnitude of elicited conformational
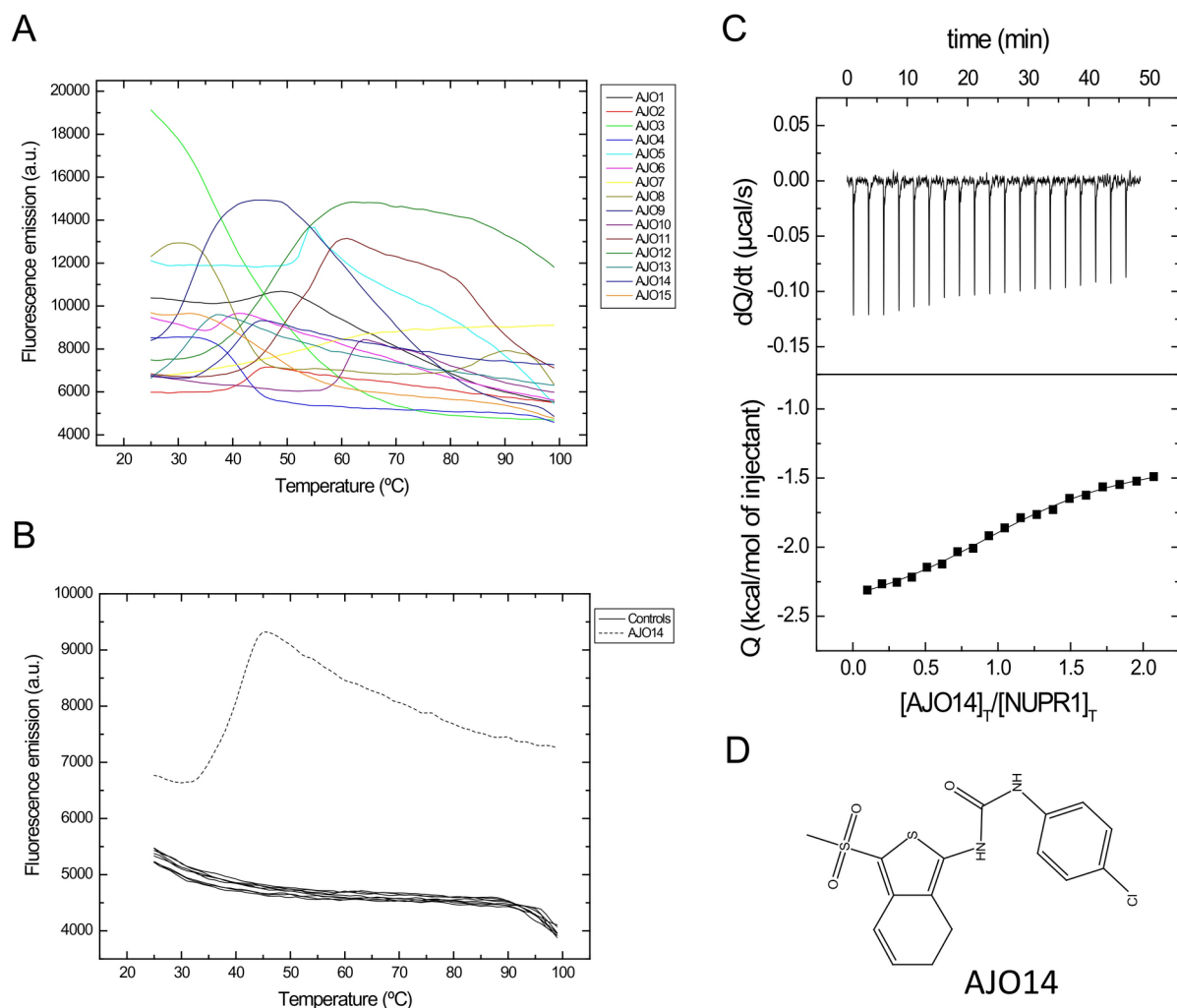
Fig. 1. In vitro molecular screening of compounds based on thermal denaturations of NUPR1. (**A**) Thermal denaturation profiles of selected compounds capable of interacting with NUPR1, and altering its thermal denaturation profile. (**B**) Regarding the subsequent assays and for a more detailed look, the most promising compound of the screening is shown (with the thermal denaturation profile of AJO14 indicated as a dashed line). The typical thermal denaturation profiles obtained from control samples (NUPR1 with no compound) are also shown (continuous line). (**C**) Calorimetric titration for AJO14 interacting with NUPR1: thermogram (upper panel) and binding isotherm (lower panel). Non-linear fit according to a model considering a single ligand binding site (continuous line) is shown. (**D**) Structure of the synthesized AJO14 compound.

changes or rearrangements, and ligand binding affinity, meaning that compounds capable of inducing a larger stabilization effect in NUPR1 do not necessarily show a higher binding affinity. Furthermore, it is possible to observe an increase in protein stability as a result of unspecific interactions between the compound and the protein, as well as interference from intrinsic compound properties (i.e., fluorescence emission, or emission in the visible spectrum in the case of a colored compound, or temperature-dependent aggregation, etc.). Therefore, ITC assays were performed to directly determine the association constants of the selected compounds. We performed ITC assays for all the compounds of the AJO series at 15 °C and pH 7 (Table 1). However, considering the results of the subsequent assays described below, only the calorimetric titration of AJO14 is shown (Fig. 1C). The dissociation constant was in the low micromolar range, indicating that AJO14 (Fig. 1D) would constitute a good starting point for further structural and functional optimization.

Identification of the binding regions of NUPR1 and AJO compounds by NMR

We aimed to verify whether the binding regions in NUPR1 of the AJO compounds series were the same as those observed for other NUPR1-binding compounds previously described[17,18]. Thus, 2D^{1}H-^{15}N-HSQC NMR experiments were carried out with ^{15}N-labeled NUPR1 (Table 2). For all compounds, we found that there were no changes in the chemical shifts of the cross-peaks of NUPR1, but variations were observed in their intensities upon addition of the corresponding compound. This indicated that NUPR1 remained mainly disordered (i.e., forming fuzzy complexes) upon binding to the compounds, and no new secondary or tertiary structures were acquired. The protein residues whose cross-peak intensities were affected upon addition of each compound are

Compound	K_a (M^{-1})	K_d (µM)	ΔH (kcal/mol)	n
AJO1	1.2×10^5	8.5	− 5.2	1.3
AJO2	0.29×10^5	35	− 10.0	1.3
AJO3	–	–	–	–
AJO4	0.44×10^5	23	1.1	1.4
AJO6	0.19×10^5	51	− 2.2	1.1
AJO7	0.11×10^5	93	5.0	1.0
AJO8	1.2×10^5	8.3	1.4	1.1
AJO9	1.4×10^5	7.1	0.6	1.3
AJO10	0.88×10^5	11	− 0.7	1.0
AJO11	0.26×10^5	38	1.5	1.0
AJO12	2.5×10^5	4.0	0.9	1.1
AJO13	0.50×10^5	20	0.7	0.9
AJO14	2.0×10^5	4.9	− 1.2	1.2
AJO15	0.84×10^5	12	1.3	1.3

Table 1. Interaction parameters of the NUPR1-AJOs complexes obtained by ITC at 15 °C and pH 7. Relative error in K_a and K_d is 20% Absolute errors in ΔH and n are 0.5 kcal/mol and 0.2, respectively.

indicated in Table 2. Ser31 was the amino acid identified as most frequently affected by the binding of the whole set of compounds, in correspondence with the well-known Ala33 hot-spot binding region of NUPR1[17,18]. Thus, we concluded that there was binding between the compounds and NUPR1.

Compound AJO14 is a specific and effective NUPR1 inhibitor with a strong antitumoral effect

The selected 14 compounds were tested for anticancer activity in the human PDAC cell line (MIA PaCa-2) using PrestoBlue™ cell viability assay. Among these small molecules, AJO3, AJO7, and AJO14 showed the best antiproliferative activity (Fig. 2A and Table S1). However, it is worth noting that the anticancer activities of these compounds were not as effective as our previously discovered NUPR1 inhibitor ZZW-115[18]. Next, in order to verify that these compounds exerted anticancer activity by targeting NUPR1, we tested their cytotoxicity on PDAC cell lines with wild-type NUPR1 (NUPR1-WT) or with the protein inactivated by the CRISPR-Cas9 system (NUPR1-KO). As shown in Fig. 2B, the anticancer activity of compound AJO14 on NUPR1-WT cells was 2 to 3 times better than that on NUPR1-KO cells, whereas AJO3 or AJO7 showed a similar antiproliferative activity on the engineered cells (Table S3). Therefore, AJO14 was the most likely compound to test as being capable of exerting anticancer effects by binding to NUPR1.

Meanwhile, we tested the antitumor activity of AJO14 on 11 primary PDAC-derived cell lines and found that it exhibited potent activity against pancreatic cancer cells, with IC$_{50}$ values in the range of 10.6–23.7 µM (Fig. 2C). As NUPR1 was also highly expressed in various cancer cells, we evaluated the antitumor activity of AJO14 on HepG2 (hepatocarcinoma), MDA-MB-231 (breast cancer), H358 (lung cancer), A375 (melanoma), HT29 (colon cancer), U87 (glioblastoma), U2OS (osteosarcoma), and PC-3 (prostate cancer). The results indicated that AJO14 could effectively kill these cancer cells (Fig. 2D). In summary, AJO14 was an effective molecule for killing cancer cells by targeting NUPR1.

Compound AJO14 displayed very low hERG binding ability

In the course of developing new drugs, one of the main factors contributing to drug attrition in development, and then, their withdrawal from the market is the occurrence of cardiac arrhythmias, which is among the most common and severe side-effects. This failure is primarily associated with the inhibition of the hERG channel by the drug. Until now, and to the best of our knowledge, 17 FDA-approved drugs have been withdrawn from the market because they block the hERG channel[25,26]. Hence, early identification of compounds with hERG inhibitory properties is very important. We measured the ability of AJO14 to block the hERG channel using the Predictor™ hERG Fluorescence Polarization assay. We compared AJO14 with E-4031, a positive control, as well as with our previous NUPR1 inhibitor, ZZW-115. The IC$_{50}$ values of E-4031, ZZW-115 and AJO14 were 0.06 µM, 2 µM and more than 80 µM, respectively (Fig. 3). AJO14 showed a 1000 times lower inhibitory effect than E-4031 against hERG. Moreover, AJO14 showed much lower hERG binding ability compared to ZZW-115. Based on these findings, AJO14 is unlikely to cause cardiotoxicity related to hERG binding.

Compound AJO14 kills pancreatic cancers by combining several cell death mechanisms

After proving that AJO14 could effectively kill cancer cells (Fig. 2), we proceeded to investigate the specific cell death mechanisms involved in its mode of action. Based on the previous results obtained with ZZW-115[18], we first suspected that AJO14 could induce necroptosis and apoptosis in cancer cells. These possibilities were explored by testing LDH release and caspase 3/7 activity, respectively, at different time points. The AJO14-treated MIA PaCa-2 cells significantly increased LDH release compared with the control group, and in a concentration- and time-dependent manner (Fig. 4A). Similarly, the caspase 3/7 activity of AJO14-treated MIA PaCa-2 cells was stronger than that of the control group (Fig. 4B). Taken together, these results demonstrated that AJO14 can exert pro-necrotic and pro-apoptotic effects. We next measured cell apoptosis by flow cytometry

Compounds	Resonances
ZZW-115	A2, S9(S22), Q12, G16, E18, S23(N53), S27, L29, Y30, S31, G40, T46, A50, S58, G60, E63, N72
AJO1	S1, T4, T8, S9(S22), A11, Q12, G16, E18, S27, Y30, G39, G40, G41, G60, T68, S73
AJO2	S1, A2, T4, T8, S9(S22), A11, Q12, G16, E18, S27, L29, S31, G38, G39, G40, A50, S58, G60, G61, H62, E63, S
AJO3	T8, S31, G79
AJO4	S31
AJO6	S1, T4, T8, S9(S22), A11, Q12, G16, E18, S27, Y30, S31, H34, G40, S58, G61, H62, S73
AJO7	S1, T9, Q12, L29, S31, G40, G41,
AJO8	S1, A2, S9(S22), G16, E18, S23(N53), S27, S31, H34, G40, G44, T47, A50, T54, S58, H62, E63, N72, S73,
AJO9	T4, G16, E18, S27, S32, H34, G38, A50, G60, G61, T68
AJO10	S1, S31
AJO11	Y30, G39, A50
AJO12	S2, T8, S9(S22), G16, S27, S31, H34, G39, E63, S73
AJO13	S1, E19, L29, G40, H62
AJO14	T8, Q12, S27, Y30, S31, A33, G39, G40, G41, T46, A50, S58
AJO15	T9, Q12, S27, S31, G39, G40, G41, T46

Table 2. NUPR1 residues whose cross-peaks were affected by compound (AJOxx and ZZW-115 as a control) binding (changes in relative intensity with respect to R82).
[a]The color indicates the changes of the relative intensity of cross-peaks: $0.10 = \Delta I < 0.20$, $0.20 = \Delta I < 0.30$, $\Delta I > 0.30$. Residues within parenthesis indicate signal overlapping.

with annexin V/PI double staining. MIA PaCa-2 cells treated with AJO14 exhibited a powerful pro-apoptotic effect in a time- and concentration-dependent manner (Fig. 4C). After MIA PaCa-2 cells were treated with 80 μM AJO14 for 72 h, the proportion of apoptotic cells (early apoptosis and late apoptosis) reached 90.54%, whereas for the control group it was only 4.1% (Fig. 4D). Interestingly, pretreatment of MIA PaCa-2 cells with Z-VAD-FMK, a well-known pan-caspase inhibitor, Olaparib (a PARP inhibitor) that prevent parthanatos cells death, or Necrostatin (Nec-1), a necroptosis inhibitor, partially improved the cell viability of cancer cells treated with AJO14 (Fig. 4E). Remarkably, similar results were obtained on three primary human PDAC-derived cells (PDAC024T, PDAC054T, and PDAC084T) as presented in Supplementary Fig. 1. These results further indicated that AJO14 could induce cancer cell death by necroptosis, parthanatos, and apoptosis.

Treatment with compound AJO14 induced energetic metabolic failure by inducing a mitochondrial catastrophe

Intracellular ATP produced in mitochondria plays an important role in cell death[27]. In this regard, we tested the intracellular ATP content in MIA PaCa-2 cells after 24, 48 and 72 h of treatment with different concentrations of AJO14. Remarkably, we observed that ATP levels decreased significantly in a concentration-dependent manner upon AJO14 treatment (Fig. 5A). Accordingly, we investigated whether reduced intracellular ATP production was the result of mitochondrial dysfunction. We further examined the oxygen consumption rate (OCR) for assessing OXPHOS activity at the mitochondria by using the Seahorse XFe system. As expected, AJO14-treatment induced a significant decrease in both basal and maximal respiration, as well as reduced the oxygen consumption
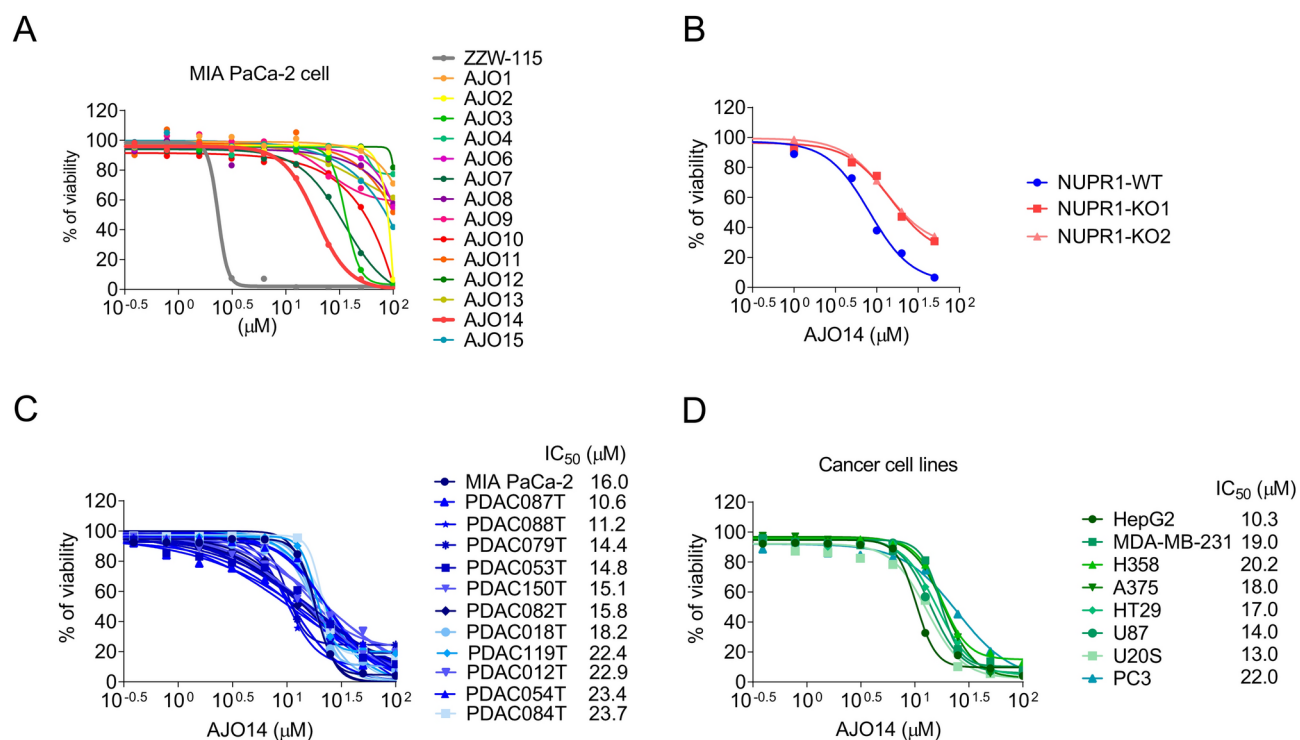
Fig. 2. AJO14 inhibited PDAC cells proliferation in vitro due to interaction with NUPR1. (**A**) Viability upon a treatment for 72 h with AJO compounds in MIA PaCa-2 cells. (**B**) Viability of AJO14 on one NUPR1-WT clone and two NUPR1-KO clones treated for 72 h. (**C**) Viability of 11 primary patients-derived PDAC cell lines treated with AJO14 for 72 h. (**D**) Viability of cell lines HepG2, MDA-MB-231, H358, A375, HT29, U87, U2OS and PC-3 at increasing concentrations of AJO14 (n = 3).

for ATP production (Fig. 5B). To further prove that mitochondrial dysfunction was linked to a process involving PARP overactivation and a consequent hyperPARylation that promoted parthanatos cell death, as previously was found upon ZZW-115-treament[28], we studied the OXPHOS activity after treatment with AJO14 either in isolation or in combination with the PARP inhibitor, Olaparib. As shown in Fig. 5C, Olaparib could reverse the strong mitochondrial metabolism failure caused by AJO14. Altogether, these results proved that AJO14 treatment induced metabolic failure with a decrease in ATP production which could be rescued by Olaparib.

Compound AJO14 inhibited PDAC tumor development in animal models

Next, our aim was to test the anticancer activity of AJO14 in vivo by using MIA PaCa-2 cells in a xenografted mouse model, as previously described. When tumors reached a volume of 200 mm^3, mice were daily treated with 5, 10, 20 and 50 mg/kg AJO14 for up to 28 days by intraperitoneal injection. The control group was treated with the corresponding volume of the vehicle, sunflower seed oil. The tumor volumes in the control group increased exponentially during these 28 days (from 222.0 ± 18.2 to 1,589.2 ± 183.1 mm^3). In contrast, mice treated with a 50 mg/kg dose of AJO14 showed slow tumor growth and a significantly reduced tumor volume compared to the control group (from an initial volume of 246.4 ± 47.7 mm^3 to final volume of 224.98 ± 53.65 mm^3 after treatment). Moreover, the tumor growth of the other three groups treated with 5 mg/kg, 10 mg/kg and 20 mg/kg of AJO14 displayed a clear dose dependency. In detail, the tumor size grew from 269.7 ± 107.4 to 1130.0 ± 389.8 mm^3 in mice treated with 5 mg/kg AJO14, from 222.5 ± 37.1 to 933.3 ± 199.9 mm^3 in mice treated with 10 mg/kg AJO14 and from 230.8 ± 81.9 to 858.2 ± 196.9 mm^3 in mice treated with 10 mg/kg AJO14 (Fig. 6A). These results clearly demonstrated that AJO14 effectively suppressed tumor growth in a dose-dependent manner. Additionally, in mice administrated with AJO14, regardless of the dose, there was no weight loss or obvious side-effects (Fig. 6B). Furthermore, a lower number of Ki-67 positive cells, a greater number of cells expressing cleaved-caspase-3, as well as higher number of TUNEL positive cells, were found in the tumoral tissue of the mice treated with a dose of 50 mg/kg (Fig. 6C). Altogether, these data indicated that AJO14 showed effective tumor growth regression with no adverse effect.

Cytotoxic activity of the AJO14-derived compounds

With the aim to improve the anticancer activity of AJO14, we have performed various structural modifications on this lead compound and designed 51 AJO14 derivatives for further studies. These compounds were synthesized, and their code, structures, synthetic protocol, chemistry structure, molecular weight and characterization data are presented in Supplementary Table 1. Briefly, as described in the Material and Methods section, the compounds were designed by the company EDELRIS by using as starting points: (1) the molecular architecture of AJO14 and 18 analogs (which were designed by modifying or replacing some of the substituents of the AJO14 scaffold);
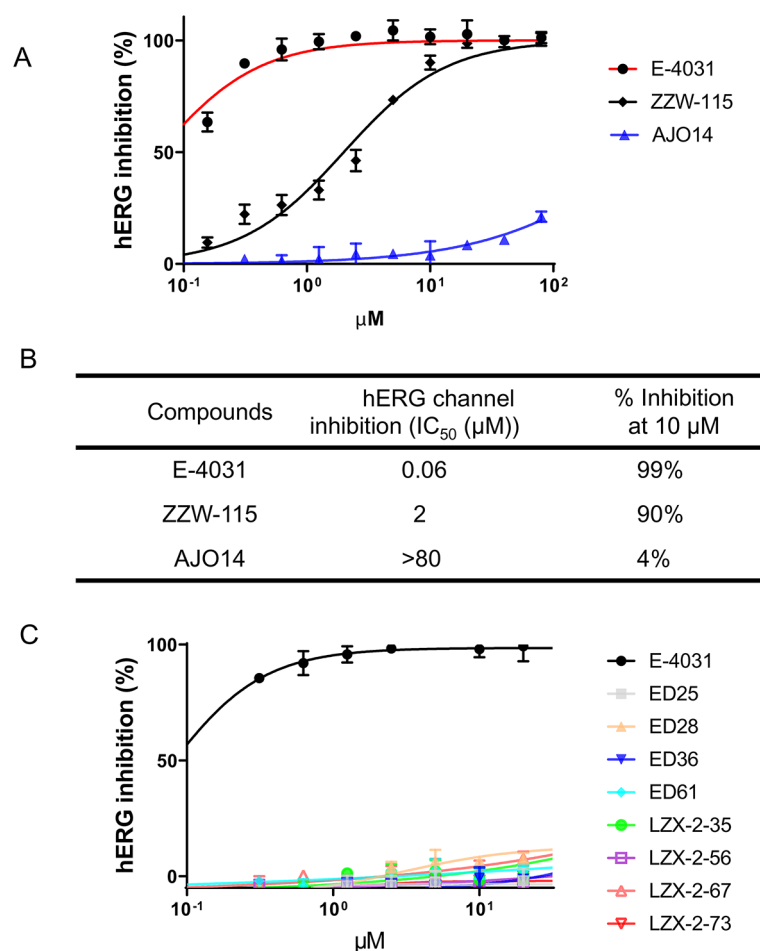
Fig. 3. AJO14 and AJO14-derivatives had low affinity for the off-target receptor hERG. (**A**) Representative graph of the concentration–response curve of E-4031, ZZW-115 and AJO14 binding to hERG, obtained by using a fluorescence polarization assay. Data are presented as mean $\pm$ SD, (n = 3). (**B**) Half-maximal inhibitory concentration (IC_{50}) values on hERG channel inhibition by E-4031, ZZW-115 and AJO14. (**C**) Representative graph of the concentration–response curve of E-4031 and selected eight AJO14-derivatives binding to hERG, obtained by using a fluorescence polarization assay. Data are presented as mean $\pm$ SD, (n = 3).

and (2) the measured IC_{50} values in four different assayed cell lines of those compounds. The new designs of the compounds considered the importance of several chemical moieties in the structure, namely, the substitution of some of the hydrogens of the urea moiety; replacing or adding some electron-withdrawing groups; and, the positions of large substituents in the phenyl rings. In addition, lager alkyl or aromatic groups were added to the sulfone moiety trying to improve the IC_{50}. Finally, the metabolic stability of those initial compounds was improved by removing the double bond of the cyclohexene present in AJO14 and its initial analogs, by addition of polar substituents to the chemical structure. We treated MIA PaCa-2 cells with increasing concentrations of these compounds and found that 8 molecules (so-called ED25, ED28, ED36, ED61, LZX-2-35, LZX-2-56, LZX-2-67 and LZX-2-73) were more cytotoxic than their precursor AJO14. The IC_{50} values were calculated for each drug (Table 3). Then, the cytotoxicity of these eight improved compounds was tested on several PDAC-derived as well as on other cancer cell lines, and confirmed their higher antitumoral effect compared to AJO14 on most cell lines (Table 4). Subsequently, we tested the hERG affinity of these eight compounds. The results, as shown in Tables 3 and 5, indicated that compounds LZX-2-73 and ED25 exhibited the lower hERG affinity and IC_{50}.

LZX-2-73 was a promising candidate to be utilized against PDAC

LZX-2-73 was selected because it was more active than AJO14 and did not bind to hERG. We started the description of its features by measuring its affinity to NUPR1 by ITC assays at 15 °C and pH 7 and found that the K_d (the dissociation constant, the inverse of the association one, K_a) was lower than its precursor AJO14 (Fig. 7) which might explain its more efficient cytotoxic activity. Then, we evaluated its anticancer effect in vivo by using MIA PaCa-2 cells in a xenografted mouse model, described above. As presented in Fig. 8, intraperitoneal administration of 5 or 25 mg/kg of LZX-2-73 showed slow tumor growth and a significantly reduced tumor volume compared to the control group in a dose-dependent manner. In summary, LZX-2-73 was more efficient than AJO14 in vitro and in vivo, and it was bound strongly to NUPR1.
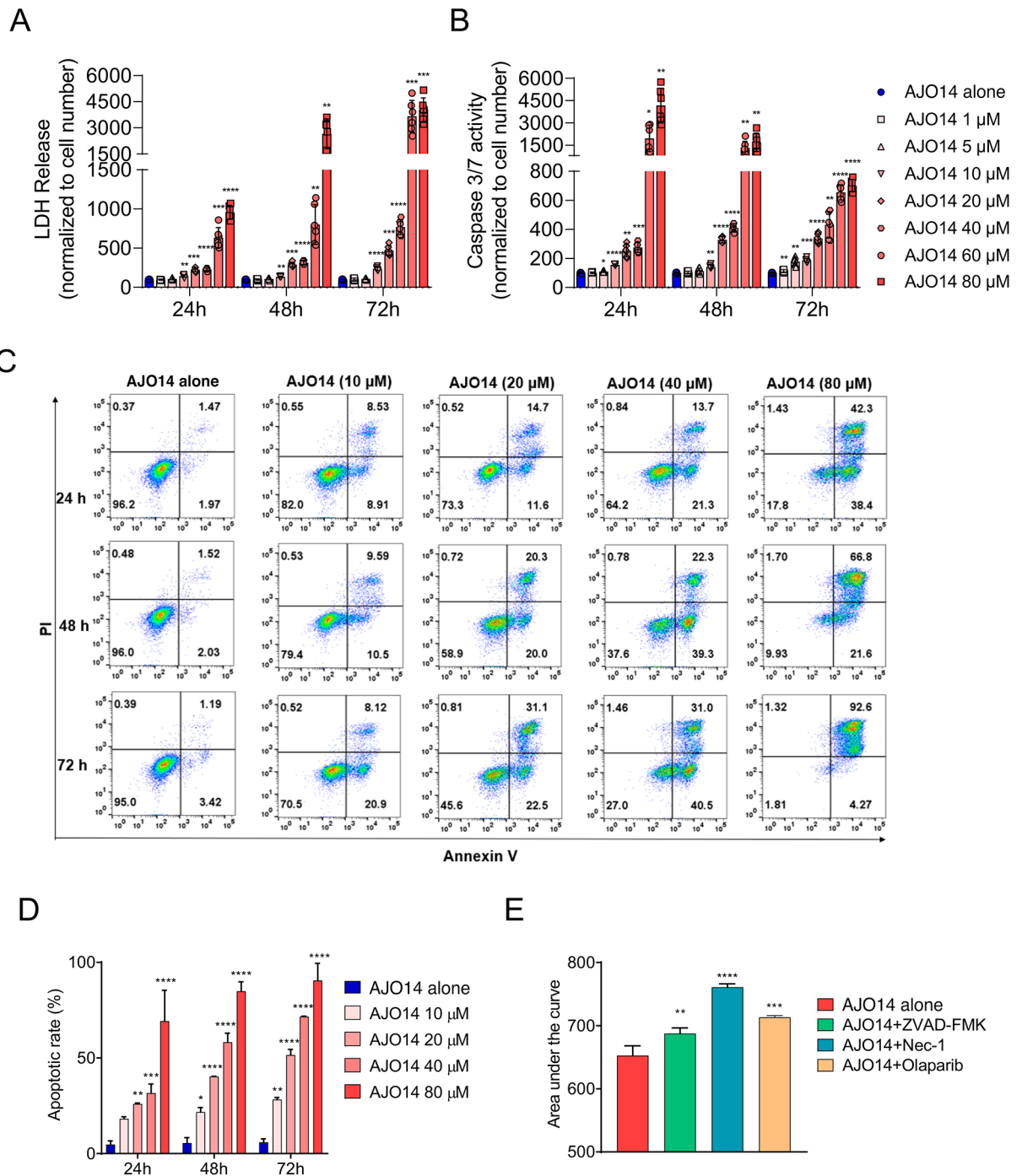
Fig. 4. AJO14 induced cancer cell death by necroptosis, apoptosis, and parthanatos. (**A**) LDH release and (**B**) caspase 3/7 activity measured on MIA PaCa-2 cells treated with increasing concentrations of AJO14 for 24, 48 and 72 h. *$p < 0.05$, **$p < 0.01$, ***$p < 0.001$, ****$p < 0.0001$ (2-way ANOVA, Dunnett's test) (n = 3). (**C**) Flow cytometry analysis of annexin/PI staining following 24, 48 and 72 h of treatment with AJO14. A representative experiment of the dot plot profile of cells is shown (n = 3). (**D**) Apoptotic rate, as the sum of the early apoptotic proportion and the late apoptotic/necrotic proportion were calculated *$p < 0.05$, **$p < 0.01$, ***$p < 0.001$, ****$p < 0.0001$ (2-way ANOVA, Dunnett's test). (**E**) Viability upon a 24 h period of treatment with increasing concentrations of AJO14 in MIA PaCa-2 cells in the presence or absence of Z-VAD-FMK (20 μM), Nec-1 (40 μM), or Olaparib (25 μM). **$p < 0.01$, ***$p < 0.001$, ****$p < 0.0001$ (1-way ANOVA, Dunnett's test) (n = 3).

Modeling the interaction of NUPR1 with LZX-2-73

The main hot spot of NUPR1 for the binding of any type of molecular partners is located around residue Ala33[29]. Other regions of this IDP are sometimes involved in the binding of drug-like compounds, the most common one being centered around Thr68[30]. The binding to all these regions is known to be governed by interactions that
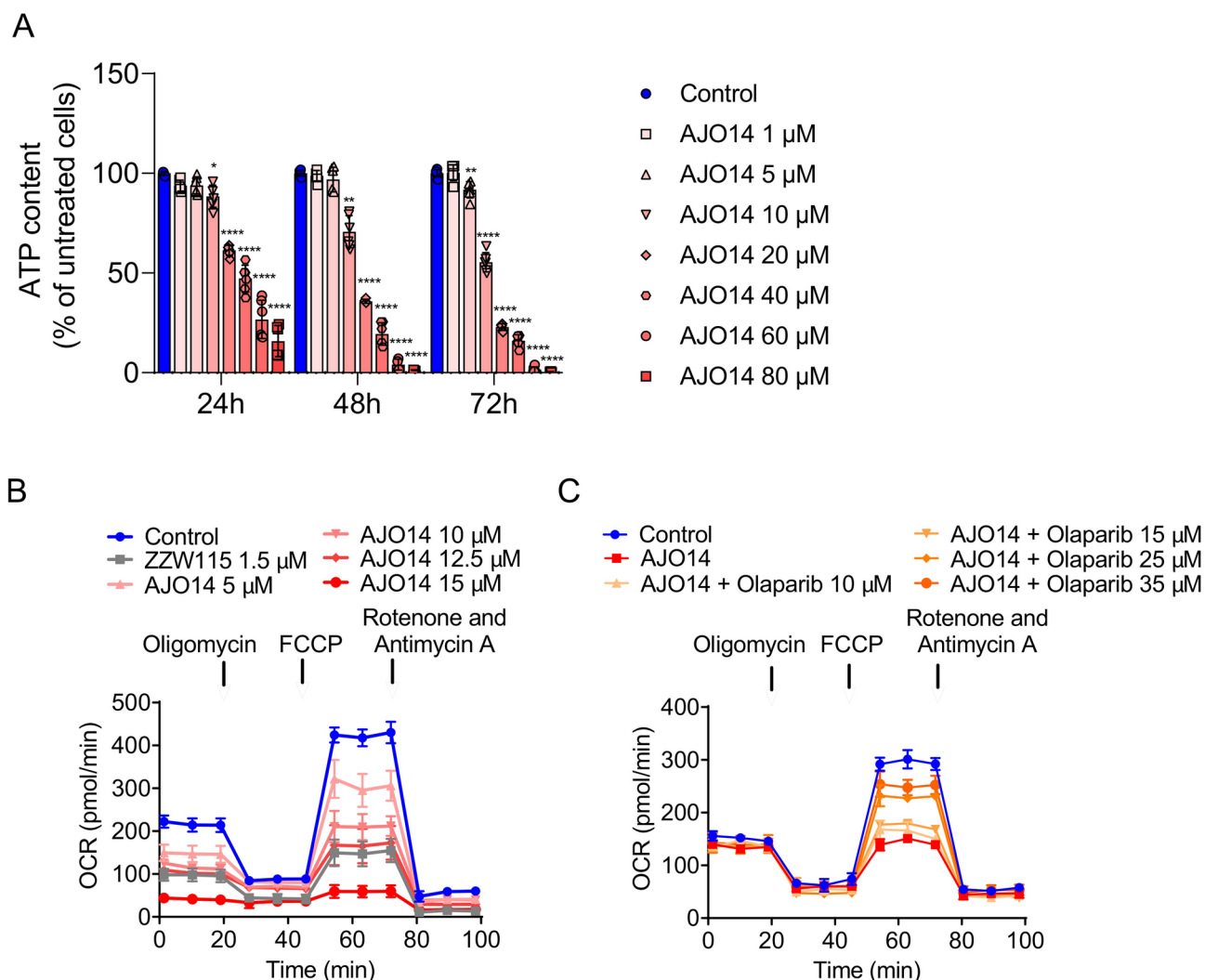
Fig. 5. AJO14 treatment induced mitochondrial metabolic failure. (**A**) Total ATP content measured in MIA PaCa-2 cells incubated with AJO14 for 24 h. *$p < 0.05$, **$p < 0.01$, ***$p < 0.001$, ****$p < 0.0001$ (2-way ANOVA, Dunnett's test) (n = 3). (**B** and **C**) Oxygen consumption rate measured in MIA PaCa-2 cells using a Seahorse XF bioanalyzer after 24 h of treatment with increasing concentrations of (B) AJO14, and in the presence of AJO14 (10 μM) with increasing concentrations of (C) Olaparib. A representative experiment is shown (n = 3).

have an essentially local character, restricted to a narrow range of about 5–7 consecutive amino acid residues along the sequence of NUPR1[17]. All these notions were exploited here to simplify our calculations, which were performed by using the docking engine AutoDock Vina[31] with its original scoring function[32]. In fact, the binding of the compound LZX-2-73 was assessed by docking it to the 5-residue fragment S[31]LAHS[35] (centered around residue Ala33, and including the key residue Ser31) of the sequence of NUPR1, either alone or in combination with another 5-residue fragment, as shown in Fig. 9.

In a first stage, the binding of LZX-2-73 to the sole sequence fragment S[31]LAHS[35] was considered (Fig. 9A). The results indicated a modest affinity, about −3.5 kcal/mol, which was markedly less favorable compared to that observed for other known compounds capable of binding to NUPR1 in the same protein region[17,18]. The main contribution to the binding energy was due to the formation of weak hydrogen bonds with poor geometry, involving the backbone of NUPR1 and the urea moiety located in the central region of LZX-2-73 (Fig. 7A); as noted above, the urea moiety was one of the regions altered upon design of the analogs. A similarly small affinity could also be obtained in some docking poses forming weak hydrogen bonds with other regions, or even lacking any specific interaction except steric contacts between the two molecular species. However, the docking score calculated in this first simulation experiment would correspond to a dissociation constant in the millimolar range, and would lead to little or no specificity in the binding of this ligand. Therefore, the most reasonable explanation to account for the binding of LZX-2-73 to NUPR1 observed in our wet-laboratory experiments is that at least a second region of NUPR1 is involved in the binding. To model this occurrence, the presence of a second fragment of NUPR1 was considered, centered around others of its known hot spot binding residues[17]. During such simultaneous docking of multiple flexible molecular species (the ligand and two protein fragments), in most docking poses, the two NUPR1 fragments were found to closely interact with each other.
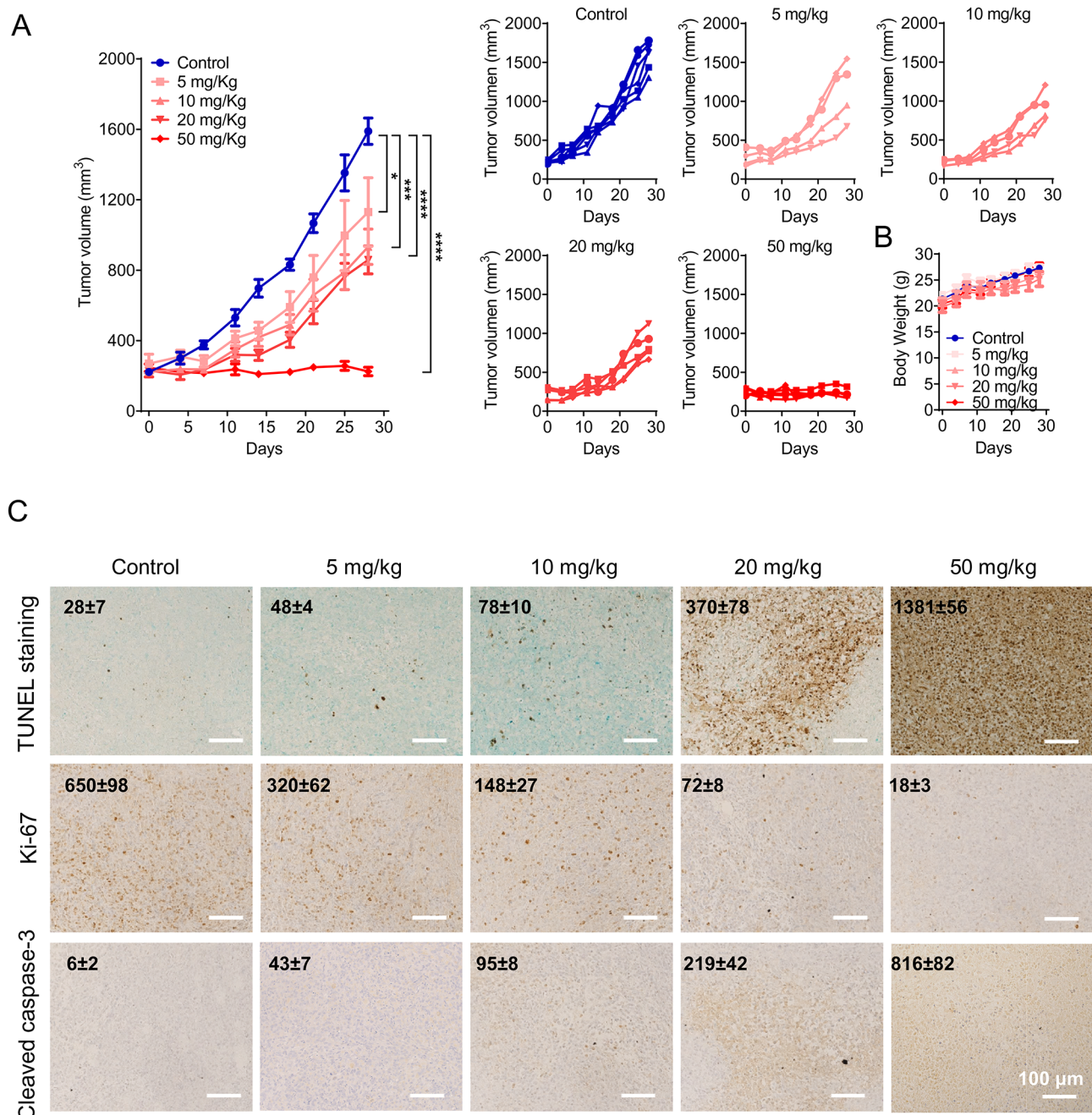
Fig. 6. Antitumoral effect induced by AJO14 treatment in vivo. Results on Crl:NU(Ico)-*Foxn1^nu* mice bearing pancreatic cancer MIA PaCa-2 cell lines xenograft treated daily with the vehicle or 5, 10, 20 or 50 mg/kg AJO14 via intraperitoneal injection (n = 5). (**A**) Tumor volume and (**B**) mice body weight were measured twice per week. *$p < 0.05$, ***$p < 0.001$, ****$p < 0.0001$ (1-way ANOVA, Dunnett's test). (**C**) Representative images of tissues sections after TUNEL, Ki-67 or cleaved caspase-3 IHC staining of tumor tissues (n = 5) (scale bar: 100 μm).

This corresponds to a realistic situation, as self-interactions among different regions of the sequence are frequent in the solution heterogeneous ensemble of an IDP, but it does not correspond to the formation of a favorable transient binding pocket for the anchoring of the ligand.

Nevertheless, we also observed docking poses in which the ligand was sandwiched in between the two protein fragments. In the most favorable model (Fig. 9B), the second NUPR1 fragment was L^66VTKL^70, which contributed to the binding by providing additional hydrophobic contacts to LZX-2-73. In this case, the binding energy reached −8.2 kcal/mol, which is slightly less favorable than the one we had previously obtained by applying a similar protocol to study NUPR1 binders synthesized from the molecular scaffold of trifluoperazine and validated by various experimental techniques[18,19]. In addition, an analysis performed by using the MM-

Compound	IC$_{50}$ (μM)	Compound	IC$_{50}$ (μM)
ED18	> 100	ED53	> 100
ED21	> 100	ED59	51.2
ED22	15.2	ED60	18.6
ED23	20.0	ED61	9.9
ED24	29.7	LZX-2-31	31.3
ED25	10.7	LZX-2-33	49.3
ED26	35.0	LZX-2-34	62.8
ED28	11.4	LZX-2-35	11.0
ED29	19.2	LZX-2-36	22.5
ED30	75.8	LZX-2-38	38.6
ED31	> 100	LZX-2-39	23.9
ED32	24.2	LZX-2-40	> 100
ED33	16.1	LZX-2-41	18.6
ED34	36.5	LZX-2-44	64.5
ED35	70.9	LZX-2-45	> 100
ED36	12.5	LZX-2-47	74.6
ED37	19.4	LZX-2-52	14.5
ED38	> 100	LZX-2-53	27.5
ED40	72.0	LZX-2-54	49.7
ED41	> 100	LZX-2-55	35.8
ED42	> 100	LZX-2-56	11.8
ED43	> 100	LZX-2-66	57.5
ED44	> 100	LZX-2-67	12.1
ED45	> 100	LZX-2-73	10.9
ED49	> 100	LZX-2-74	> 100
ED50	> 100		

Table 3. IC$_{50}$ of the 51 AJO14- derived compounds on MIA PaCa-2 cell.

| Cancer cell lines	IC$_{50}$ value (μM)								
	AJO14	ED25	ED28	ED36	ED61	LZX-2-35	LZX-2-56	LZX-2-67	LZX-2-73
PDAC021T		5.5	3.5	3.3	3.9	5.4	3.9	6.8	5.9
PDAC056T	14.5	4.3	3.2	3.7	1.9	5.3	2.9	9.1	3.4
PDAC074T	20.2	9.2	3.8	3.9	3.7	5.7	5.9	4.9	5.7
PDAC079T	14.4	6.1	5.7	2.3	3.5	3.2	2.6	2.7	3.1
PDAC087T	10.6	17.5	24.9	15.6	16.8	12.7	12.6	10.3	13.6
PDAC088T	11.2	5.7	5.7	4.2	3.8	5.6	3.5	4.3	4.2
PDAC091T		20.2	13.9	14.8	14.4	17.8	19.3	17.4	16.4
PDAC119T	22.4	10.9	6	5.1	6.1	8.5	4.4	5.4	5.1
PC3	22.0	12.0	12.0	13.1	10.0	11.4	11.5	10.6	11.6
HT29	17.0	8.9	5.5	6.7	5.5	10.5	14.8	9.6	9.7
H358	20.2	17.0	18.4	14.8	15.9	14.9	19.1	11.8	12.0
A375	18.0	8.2	8.3	9.0	5.7	14.0	9.2	14.3	9.7
U87	14.0	13.6	13.4	12.8	14.9	11.3	8.5	9.9	11.1
MDA-MB-231	19.0	11.3	13.6	10.1	11.1	10.2	13.9	9.4	9.6
HepG2	10.3	5.7	6.5	7.7	5.8	10.1	5.6	8.9	5.6
U2OS	13.0	10.5	14.4	12.5	10.4	16.2	10.0	14.4	10.0

Table 4. IC$_{50}$ of the 8 AJO14-derived compounds in different cell lines.

GBSA methodology[33] was also applied in an attempt to dissect out the individual contribution of each protein residues to the binding of the ligands, by considering multiple docking complexes obtained in simulation. The results (Supplementary Fig. 2) pointed out to minimal per-residues differences, suggesting that the binding is driven by the overall sequence of the two fragments, rather than by a single key amino acid residue.

It is worth to note that the anchoring predicted by molecular docking represents a sort of 'static' picture, which only corresponds to a qualitative model for the binding of a ligand to an IDP in solution. The docking poses

Compounds	hERG channel inhibition (IC$_{50}$ μM)	% Inhibition at 10 μM	% Inhibition at 80 μM
E-4031	0.05	97.2	100
ED25	> 80	2.8	5.4
ED28	> 80	14.7	22.0
ED36	> 80	7.5	19.2
ED61	> 80	9.2	14.8
LZX-2-35	> 80	6.9	22.6
LZX-2-56	> 80	4.7	9.5
LZX-2-67	> 80	10.0	21.6
LZX-2-73	> 80	4.4	7.1

Table 5. Half-maximal inhibitory concentration (IC$_{50}$) values for hERG channel inhibition by E-4031 and eight selected AJO14-derivatives.

B
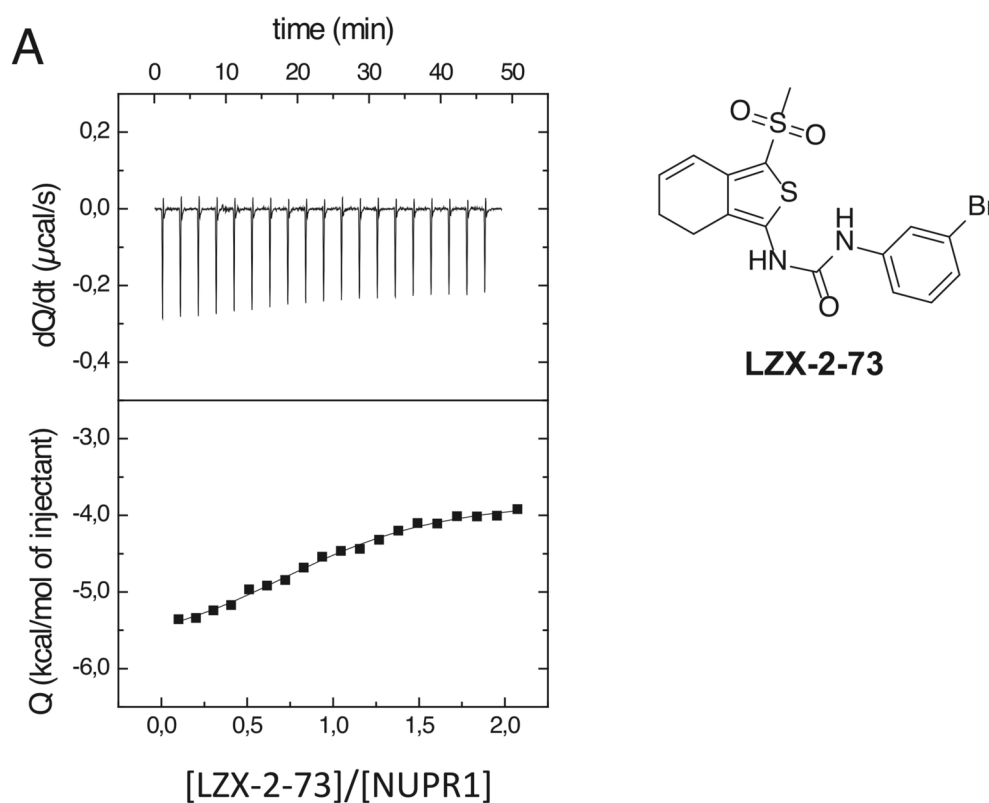
Interaction parameters of the NUPR1-LZX-2-73 complexes obtained by ITC at 15° C and pH 7.

Compound	K_a (M^{-1})	K_d (μM)	ΔH (kcal/mol)	n
LZX-2-73	$3.7 \cdot 10^5$	2.7	-2.2	0.98

Fig. 7. Calorimetric titration for LZX-2-73 interacting with NUPR1. (**A**) Thermogram (upper panel) and binding isotherm (lower panel). Non-linear fit according to a model considering a single ligand binding site (continuous line) is shown. Chemical structure of the synthesized LZX-2-73 compound. (**B**) Interaction parameters of the NUPR1-LZX-2-73 complexes obtained by ITC at 15 °C and pH 7.
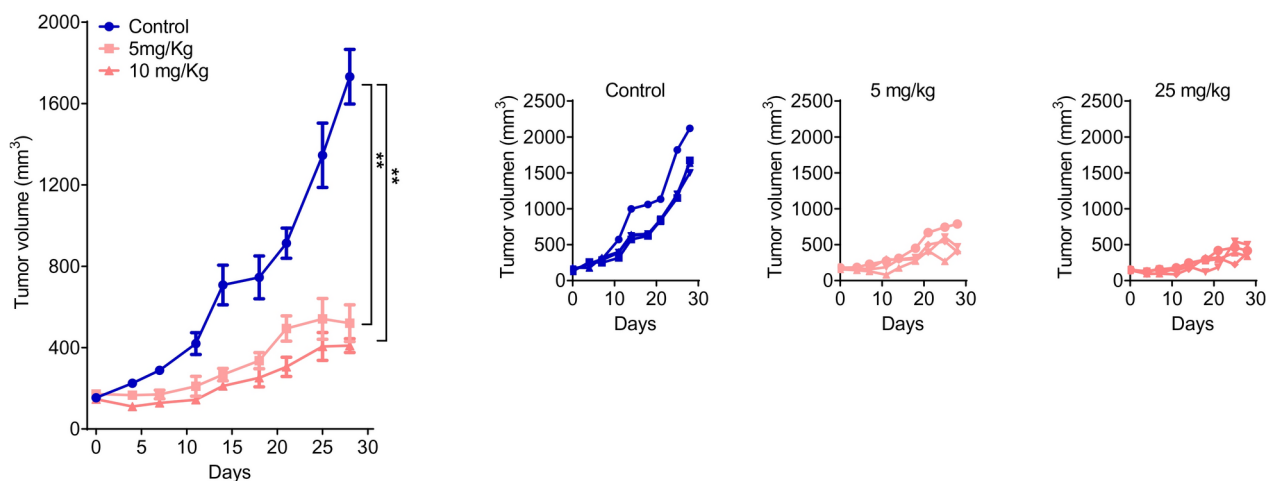
Fig. 8. Antitumoral effect induced by LZX-2-73 treatment in vivo. Results on Crl:NU(Ico)-Foxn1nu mice bearing pancreatic cancer MIA PaCa-2 cell lines xenograft treated daily with the vehicle or 5 or 25 mg/kg LZX-2-73 via intraperitoneal injection (n = 3). Tumor volume and mice body weight were measured twice per week. **$p < 0.01$ (1-way ANOVA, Dunnett's test).
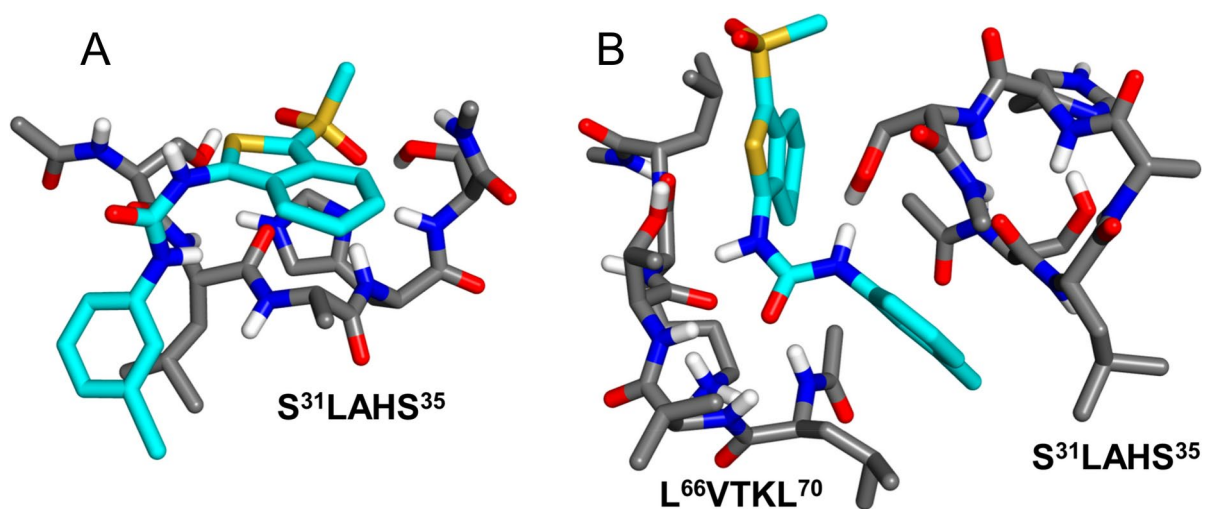

Fig. 9. Molecular docking of compound LZX-2-73 to key 5-residue fragments of NUPR1. (**A**) Most favorable pose among those predicted in the docking to the sole fragment $S^{31}LAHS^{35}$. (**B**) Most favorable pose in the simultaneous docking of both fragment $S^{31}LAHS^{35}$ and $L^{66}VTKL^{70}$.

found represent minima in the energy landscape for the bound protein/ligand complex, and the corresponding docking scores approximated the ligand affinity towards NUPR1, although is it likely that they overestimated the enthalpic component of the binding free energy of LZX-2-73.

Discussion

Pancreatic cancer is one of the most lethal and aggressive forms of cancers, marked by extremely poor therapeutic outcomes. In this challenging scenario, our research has focused on NUPR1, as a promising therapeutic target, to meet the urgent need for novel treatment strategies for PDAC. NUPR1 represents an interesting therapeutic target to treat PDAC, primarily due to its unique role in regulating key cellular processes involved in cancer progression, including cell survival, proliferation, and stress response. Our findings, along with existing literature, highlight NUPR1's overexpression in PDAC and its essential contribution to tumor growth and resistance to traditional therapies, positioning it as a critical lever for intervention in pancreatic cancer treatment. This IDP was first described as being activated in the exocrine pancreas in pancreatitis[34], an inflammatory disease that, in its chronic form, behaves as a preneoplastic condition for PDAC development. Importantly, NUPR1 was found to be overexpressed in many cancerous tissues, in which its constant expression is essential for the tumor development and progression[18]. In validating the essential role of NUPR1 in PDAC, our study employed a genetic inhibition approach by using siRNA, which not only corroborated previous findings regarding NUPR1 involvement in

cancer progression, but also provided new insights into its multifaceted role within pancreatic cancer cells. Furthermore, our observation that tumors treated with NUPR1-targeted siRNA ceased their progression[12] offers compelling evidence of NUPR1 as a viable therapeutic target, providing a more nuanced understanding of its function and potential for targeted therapy in PDAC. Other research groups, by using siRNA against NUPR1, demonstrated that inactivation of NUPR1 induced cell death and arrest of the tumoral growth on hepatocellular carcinoma and cholangiocarcinoma, non-small cell lung cancer, osteosarcoma, multiple myeloma, glioblastoma, ovarian cancer, and face and neck cancer, corroborating the notion that NUPR1 is a promising target for PDAC, and probably for many other cancers[35–37].

Previous results obtained by using circular dichroism (CD) and NMR showed that NUPR1 is completely disordered along its whole sequence[38]. Therefore, classical approaches for the experimental screening of compounds to identify inhibitors cannot be applied. The structure of NUPR1 cannot be solved by crystallography or cryo-electron microscopy, or be predicted by homology modeling or other more sophisticated computational techniques; in fact, an IDP in solution spans a statistical ensemble of highly disordered conformations, therefore a single representative structure does not even exist. However, when a ligand interacts with a protein, even one as intrinsically disordered as NUPR1, this interaction might induce localized and limited structural rearrangements, potentially altering the protein thermal denaturation pattern. Our approach, leveraging TSAs with the extrinsic fluorescent probe ANS, represents a significant advancement over traditional screening methods. By focusing on changes in thermal stability as a proxy for binding, we have successfully identified compounds that interact with NUPR1, overcoming the challenges posed by its disordered structure. This method not only enhances the sensitivity of our screening process but also allows for the identification of ligand-induced structural changes that might not be detectable through conventional means. Our innovative application of TSA to the study of NUPR1, thus, opens new pathways for the discovery of therapeutic agents targeting IDPs, a class of proteins traditionally considered challenging due to their dynamic nature. By using a fluorescence thermal denaturation method, we screened 10,000 compounds and found that 15 of them (14 with acceptable solubility) could bind to NUPR1. Among these compounds, AJO14 was identified as the most promising candidate, with superior cytotoxic activities both in vitro and in vivo against PDAC, compared to the other molecules identified. Additionally, AJO14 showed very low hERG affinity, and consequently, a reduced risk of cardiotoxicity. We pinpoint that AJO14 promotes cell death through necroptosis, apoptosis, and parthanatos, all mechanisms associated with a severe mitochondrial catastrophe induced by an uncontrolled hyperPARylation[28,38–40], which, in turn, triggers a reduction in ATP production. We have previously demonstrated through proteomic, cellular, and biochemical analyses that NUPR1 binds to and inhibits PARP1 activity in the nucleus. Mutations at Ala33 or Thr68 of NUPR1 block this effect, enhance PARylation induced by DNA-damaging agents, decrease the $NAD^+/NADH$ ratio, and are reversed by the PARP inhibitor olaparib. Pharmacological inhibition of NUPR1 induces cell death in pancreatic cancer cells, an effect reversed by olaparib and enhanced by the PARG inhibitor PDD00017273. Notably, genetic inactivation of NUPR1 causes mitochondrial catastrophe, characterized by hyperPARylation of mitochondria, disorganized mitochondrial networks, decreased mitochondrial membrane potential, and increased levels of superoxide, reactive oxygen species (ROS), and cytosolic Ca^{2+}. These effects are mitigated by olaparib, NAD + precursor nicotinamide mononucleotide, and partially by antioxidants. Consequently, although NUPR1 inhibitors were developed to combat pancreatic cancer, this strategy is not recommended in the 5% of patients with BRCA mutations, for whom olaparib is indicated.

All these functional characteristics are similar to those obtained by genetic inactivation of NUPR1[12], or by treatment with the previously-identified NUPR1 inhibitor ZZW-115[18], indicating that AJO14 binds to NUPR1 and inactivates it. Furthermore, we obtained 51 derivatives of AJO14 by performing molecular modification to improve its anticancer activity and physicochemical properties. Among these variants, eight compounds showed a notable gain in efficacy, when compared to AJO14.

It is interesting to note that, due to the modifications we have done, there is no particular similarity between the molecular scaffold of AJO14 (and its derived compounds) and the other compounds previously identified as inhibitors of NUPR1[17], including ZZW-115 and its analogues[18]. Our docking experiments on LZX-2-73 provide some subtle but clear indications that transient hydrogen bonds and local hydrophobic contacts are the main determinants driving the association of these new compounds to NUPR1. Furthermore, anchoring to the sole hot spot region around Ala33 is not sufficient to ensure the binding of this compound, and the participation of a second region of NUPR1 is necessary. In this respect, the most favorable one appears to be the region around residue Thr68. However, other important molecular details that determine the interaction to NUPR1 remain still elusive. Even considering the most favorable anchoring location identified in simulation, LZX-2-73 does not show an affinity for NUPR1 higher than most other inhibitors[18]. Thus, the increased efficiency of AJO14 and its derived compounds cannot be ascribed to a more favorable binding energy. This observation confirms that for NUPR1 the best drug is not necessarily the best binder, in agreement with our previous studies[17,18]. In fact, since this protein performs multiple functions within cells (as most IDPs do), an improved affinity in vitro may not necessarily correspond to a larger inhibitory effect in the cells. In addition, intrinsic and specific drug-dependent pharmacokinetic factors may play a crucial role in determining the best drug. This observation poses some further serious challenges on how to select new scaffolds, or improve the ones already identified. While our findings present AJO14 and its derivatives as promising NUPR1 inhibitors with potent anticancer activity and minimal cardiotoxicity risks, it is imperative to acknowledge the limitations of our current study. Specifically, the potential for undetected off-target effects remains an important consideration. The identification of such off-target interactions is crucial for fully understanding the therapeutic profile and safety of these compounds. To address this, future research should include comprehensive pharmacological profiling and in-depth mechanistic studies, aimed at elucidating the full spectrum of molecular interactions these compounds may engage in. Additionally, advanced in vivo models and patient-derived xenografts could provide further insights into the efficacy and safety of these inhibitors in a more clinically relevant context. By pursuing these investigational

avenues, we aim to refine our understanding of AJO14 and its analogs mechanism of action, optimize their therapeutic potential, and ensure their safety profile is thoroughly characterized before clinical application.

In conclusion, our research underscores the significant potential of AJO14 and its derivatives as breakthrough options for the treatment of PDAC, a disease that has long challenged the medical community with its dismal prognosis and limited treatment options. By targeting NUPR1, a protein pivotal to the survival and proliferation of cancer cells, these compounds offer a novel and promising approach to overcoming some of the most persistent obstacles in PDAC therapy. The innovative mechanism of action, coupled with a reduced risk of cardiotoxicity, positions AJO14 as a frontrunner in the development of more effective and safer cancer treatments. However, while our study lays a solid foundation for the therapeutic exploitation of NUPR1, it also opens up new avenues of investigation. Questions regarding the comprehensive understanding of off-target effects, the optimization of compound efficacy through structural modifications, and the translation of these findings into clinical success remain to be fully addressed. The journey from bench to bedside is complex and requires not only continued innovation and rigorous testing but also a multidisciplinary effort to ensure that the promise of AJO14 and its derivatives is fully realized for patients suffering from pancreatic cancer.

Material and methods

Recombinant NUPR1 protein expression and purification
NUPR1 was produced and purified from transformed *E. coli* grown in Luria–Bertani broth (LB) medium as previously described[38].

Chemical libraries
The HitFinder Chemical Library (Maybridge Company, UK), comprising a collection of 10,000 compounds from various sources and providing an extensive chemical diversity. The compounds in the library were supplied in 96-well plates, dissolved in 100% dimethyl sulfoxide (DMSO) at a final concentration of 10 mM.

Screening by thermal-shift assay (TSAs)
Potential ligands for NUPR1 were identified from the HitFinder Chemical Library by using a high-throughput screening procedure based on TSA, monitoring the ligand-induced protein stabilization against thermal denaturation by differential scanning fluorimetry. The procedure employed was similar to that used previously for identifying other small-molecule compounds that act as inhibitors of NUPR1[17]. Briefly, thermal denaturation experiments of NUPR1 in the presence of compounds were performed in a Stratagene Mx3005P real-time qPCR thermal cycler (Agilent Technologies, California, USA). The extrinsic fluorescent probe 8-anilino-1-naphthalene sulfonic acid (ANS) (Sigma Aldrich, Madrid, Spain) was used as a reporter for changes in the hydrophobicity of the protein, indicative of the binding of a ligand and reflecting conformational changes and/or exposure of protein hydrophobic surfaces induced by temperature increase. For each well of a 96-well microplate (96-Well PCR Plate, Non-skirted from 4titude), a volume of 100 µL of protein solution containing final concentrations of 4 µM NUPR1, 100 µM ANS and 250 µM of each compound (2.5% residual final concentration of DMSO) in buffer 50 mM sodium phosphate, 150 mM NaCl (pH 7.4) was dispensed. Then, the microplate was incubated at room temperature for 10–15 min before loading onto the microplate reader. Thermal unfolding curves were recorded from 25 to 100 °C, at a scanning rate of 1 °C/min. The increase in ANS emission fluorescence intensity (with excitation wavelength $\lambda_{exc} = 370$ nm, and emission wavelength $\lambda_{em} = 492$ nm) was monitored during thermal unfolding. The fluorescence intensity of ANS greatly increases when it binds to hydrophobic regions of the protein that become exposed to the solvent upon thermal unfolding and ligand dissociation. Control experiments were routinely conducted with NUPR1 samples with and without DMSO on each microplate. Hits were identified as compounds that shifted the temperature for maximal slope towards higher temperatures, compared to the internal controls in each microplate, thus inducing a stabilizing effect on NUPR1. These compounds were assumed to be potentially capable of inhibiting any subsequent protein-NUPR1 interactions. Alternatively, compounds inducing on NUPR1 a markedly different thermal denaturation pattern compared to the unliganded protein were also selected. Although NUPR1 is an IDP, binding compounds would promote local folding on NUPR1, and thermal destabilization and unfolding of that local structure would be observed in the assays.

Isothermal titration calorimetry (ITC)
A high-sensitivity isothermal titration calorimeter Auto-iTC200 (MicroCal, Malvern-Panalytical, Malvern, UK) was used for target engagement by direct assessment of the compound's interaction with NUPR1[41]. To avoid issues related to bubble formation in the cell and syringe, and to ensure a good quality of the assays, both the protein and the compound solutions were properly degassed. Experiments were performed with freshly prepared buffer-exchanged protein solutions, at 15 °C, in buffer 50 mM sodium phosphate (pH 7.0). The NUPR1 protein solution at 20 µM was titrated in the calorimetric cell by injecting a compound solution at 200 µM from the syringe through a series of 19 injections of 2 µL each, with a stirring speed of 750 rpm, and a reference power of 10 0µcal/s. The heat evolved after each ligand injection was obtained from the integration of the calorimetric signal in the thermogram (thermal power vs. time). The heat due to the binding reaction was obtained as the difference between the reaction heat and the corresponding heat of dilution, the latter being estimated as a constant value throughout the experiment, and included as an adjustable parameter in the analysis. Control experiments (compound injected into the sole buffer) were performed under the same experimental conditions, in order to observe potential unspecific phenomena (e.g., solution composition mismatches or self-association of compounds). The enthalpy change, ΔH, and the association constant, K_a, of the binding reaction were obtained through non-linear least-squares regression data analysis of the experimental binding isotherm (ligand-normalized heat effect per injection vs. molar ratio), by applying a model considering a single ligand binding site

in the protein. Experiments were performed in replicates and data were analyzed using an in-house developed software implemented in Origin 7 (OriginLab, Northampton, MA).

NMR spectroscopy

The NMR data were acquired at 25 °C, pH 4.5 (acetate buffer), on a Bruker Avance DRX-500 spectrometer equipped with a triple-resonance probe and z gradients. All spectra were referenced to external TSP as previously described[18,42]. The 2D ^{1}H-^{15}N heteronuclear single-quantum coherence (HSQC) spectra were acquired either for isolated ^{15}N-labeled NUPR1 (100 μM) or in the presence of the corresponding selected compound (400 μM). Frequency discrimination in the indirect dimensions was achieved by using the echo/antiecho-TPPI method. The spectra were acquired with 1024 complex points in the ^{1}H dimension, 128 complex points in the ^{15}N dimension, and 200 scans. The carrier of the ^{1}H dimension was set at 5.00 ppm, and that of ^{15}N was set at 120 ppm. The spectral widths used were 10 ppm and 35 ppm in the ^{1}H and ^{15}N dimensions, respectively. Water signal was suppressed with the WATERGATE sequence. Data were zero-filled to double the number of original points in both dimensions, apodized with shifted squared sine-bell functions in the 2 dimensions, and Fourier transformed with the program TopSpin 2.1. Assignments were taken from those previously reported for NUPR1[42]. The intensity of the signals from each row in the HSQC spectra was measured by using TopSpin 2.1, and considering the intensity of the last residue of NUPR1, namely Arg82, as an internal reference. Differences in intensity of a particular protein residue between spectra of the complex (NUPR1/compound) and that of isolated NUPR1 were considered significant only if greater than 10%.

Cell lines and cell culture

Cells were obtained from the ATCC. Human pancreatic cancer cells (MIA PaCa-2 and WT Panc-1), human hepatocellular carcinoma cells (HepG2), human breast adenocarcinoma cells (MDA-MB-231), human melanoma cells (A375), human colorectal cancer cells (HT29), human primary glioblastoma cells (U87), and human bone osteosarcoma epithelial cells (U2OS) were cultured in Dulbecco's modified Eagle's medium (DMEM) (Gibco, Invitrogen) containing 10% fetal bovine serum (FBS) (Biosera). Human lung carcinoma cells (H358) and human prostate cancer cells (PC-3) were cultured in RPMI 1640 medium (Gibco, Invitrogen), containing 10% FBS. Primary human PDAC cells were cultured in the serum-free DMEM/F12 medium, adding 1.22 g/L nicotinamide, 5 g/L glucose, 5% Nu-Serum IV, 0.5% ITS + Premix Universal Culture Supplement (containing insulin, human Transferrin and selenous acid), 1 μM dexamethasone, 10 ng/L cholera toxin, 50 nM 3,3′5-triiodo-L-Thyronine, 25.2 mg/L bovine pituitary extract, and 20 μg/L epidermal growth factor. Cells were cultured in a humidified incubator with 5% CO_2 at 37 °C, cell were tested mycoplasma-free. NUPR1 KO Panc-1 were developed in our laboratory[43]. Three primary human PDAC-derived cells (PDAC024T, PDAC054T, and PDAC084T) were obtained from our PaCaOmics biobanking and cultivated as previously published[44].

Cell viability assay

The cultures were plated at 5000 cells per well in 96-well plates and incubated 24 h to attach to the surface. Cells were then incubated with increasing concentrations of each compound for 72 h. Cell viability was measured after addition of the PrestoBlue™ Cell Viability Reagent for 3 h, and quantified by using the plate reader Tristar LB941. Untreated cells were used as control. All experiments were performed in triplicate.

Animals

Female Crl:NU(Ico)-*Foxn1^{nu}* mice (4 weeks old) were purchased from Charles River Company. Mice were kept in an agreed Experimental Animal House of the *Centre de Cancérologie de Marseille, pôle Luminy*. All mice were fed under specific pathogen-free conditions and handled according to the principles of the laboratory animal care and recommendations to ethics laws. Ten millions of MIA PaCa-2 cells with 50 μL Matrigel (BD Pharmingen) were inoculated subcutaneously in nude mice of 5 weeks. Mice were treated daily with 0.5% DMSO in sunflower seed oil (vehicle), and 5, 10, 20, or 50 mg/kg of compound AJO14 by intraperitoneal injection when the tumor size reached 200 mm^3. Twice per week the mice were weighed and the tumor volumes were measured with a caliper (tumor volume was calculated by assuming an ellipsoid shape). Another independent cohort of 9 animals was split in 3 groups of 3 mice/group and treated with 5 and 25 mg/kg or 0.5% DMSO. Mice were sacrificed after 28 days of treatment. The animal experiments were performed in accordance with.

hERG channel binding assay

The propensity of a given compound to block the hERG potassium channel was measured by using a Predictor™ hERG Fluorescence Polarization assay, Thermo Fisher Scientific, France, following the manufacturer protocol. Specifically, membrane fractions containing hERG channel protein were incubated with compounds to be tested at varying concentrations from 0.1 to 80 μM, and fluorescence polarization (mP) was measured and recorded. E-4031, a selective hERG potassium channel blocker, was used as the positive control in the assay. The test compounds were prepared at 100× in DMSO and then diluted them 4× (4% DMSO) in the assay buffer. The wells contained 5 μL assay buffer, while 10 μL of the hERG membrane samples were used as negative control. Then, 5 μL of the test substances were dispensed into a 384-well plate at a final concentration of 0.1–80 μM into each well. Next, 10 μL of 2× Predictor hERG membranes were dispensed into each well, followed by 5 μL of 4× Predictor hERG Tracer Red. Each substance was tested in the absence and presence of 30 μM E-4031 to correct for possible test interference. The plates were incubated for at least 7 h prior to measuring the fluorescence polarization using a BMG LABTECH (PHERAstar), at excitation and emission wavelengths of 540 and 573 nm, respectively.

LDH assay, caspase-3/7activity assay and ATP production

MIA PaCa-2 cells were seeded in 96-well plates at a density of 10,000 cells per well. Cells were allowed to adhere for 24 h and then treated with AJO14 at increasing concentrations for 24, 48 or 72 h, in triplicates. The LDH release, caspase 3/7 activity and ATP production were measured using CytoTox-ONE™, Caspase-Glo® 3/7 and CellTiter-Glo® assay (Promega, France), respectively. For LDH and caspase-3/7 activity assays, data were normalized to the cell number. In the case of the ATP assay, the data were normalized to that of untreated cells.

Annexin V/PI staining

MIA PaCa-2 cells were harvested after incubating with AJO14 for 24, 48, and 72 h. Cells were detached by Accutase (Thermo Fisher Scientific, France) and resuspended in 100 µL of Annexin-binding buffer. A volume of 5 µL of Pacific-Blue Annexin V (Biolegends, Netherlands) was added to the cell suspension and incubated in the dark for 15 min. Five min before analysis by flow cytometry, 5 µL propidium iodide (PI) was added to the cell suspension. Ten thousand events per sample were collected and analyzed by MACSQuant-VYB (Miltenyi Biotec, Surrey, UK). Data analysis was performed using FlowJo 10.7.1 software (BD, USA).

Measurement of mitochondrial oxidative phosphorylation (OXPHOS)

The measurements were conducted using a Seahorse Bioscience XF24 Extracellular Flux Analyzer (Agilent, France). MIA PaCa-2 cells were plated at 30,000 cells/well onto Seahorse 24-well plates, and incubated overnight. Cells were treated with compound AJO14, either alone or in combination with Olaparib at the indicated concentrations, for 24 h. The cellular oxygen consumption rate (OCR, in pmol/min) was measured using the XF Cell Mito Stress Test Kit (Agilent, France) under basal conditions and in response to 1 µM oligomycin (an ATPase inhibitor), 0.5 µM carbonyl cyanide p-(trifluoro-methoxy) phenylhydrazone (FCCP, a potent uncoupler of oxidative phosphorylation), and rotenone and antimycin A (0.5 µM each) (electron transport chain inhibitors).

In situ detection of apoptotic cells in tumor tissue

Four µm-thick sections were obtained from paraffin-embedded tumors using a Leica microtome (Leica Biosystems, Germany). The TUNEL apoptosis assay kit (Abcam, USA) was used to detect apoptotic cells in tumor samples, according to the manufacturer's protocol. In brief, tumor sections were deparaffinized and rehydrated before permeabilization with Proteinase K. Then, endogenous peroxidases were inactivated with 3% (v/v) H_2O_2. Apoptotic cells were labelled with TdT Enzyme that binds to exposed 3′-OH ends of DNA fragments and catalyzes the addition of biotin-labeled deoxynucleotides, biotinylated nucleotides are bound with a streptavidin–horseradish peroxidase (HRP) conjugate. The signal was detected by using 3,3′-Diaminobenzidine (DAB) substrate, which reacts with the HRP labeled sample, and the sections were counterstained with Methyl Green. To generate a negative control, TdT enzyme was replaced by distilled water in the reaction mix. Positive control was performed by treating the sample with 1 µg/µL DNase I for 20 min. Finally, a glass coverslip and mounting media were used to protect the samples. Images of the sections were taken by ZEISS Axio Imager Z2 microscope (Zeiss, Germany).

Immunohistochemistry

Immunohistochemistry staining was performed on 4 µm-thick paraffin-embedded tissue sections. After deparaffination, antigen retrieval was performed in a water bath at 96 °C, in Buffer (Citrate) TRIS at pH 6 (Dako S1699) during 20 min. Blocking of endogenous peroxidases was performed and, then, the following primary antibodies were used: rabbit anti-Ki67 (Abcam ab92742, 1:100 dilution) and rabbit anti-cleaved caspase-3 (9661; Cell Signaling Technology, 1:400 dilution). Then, an incubation for 30 min with a biotinylated secondary antibody (1:400 dilution), followed by an incubation with Streptavidin-HRP (P0397) (1:500 dilution) was performed. Signal was detected with DAB (Dako, K3468) following the manufacturer's protocol. Coloring of the samples was performed with Mayer's Hematoxylin for 30 s, followed by addition of 0.1% sodium bicarbonate solution for 3 min. Finally, samples were dehydrated and assembled with mounting media.

Design and synthesis of the AJO14-derived compounds

Based on the scaffold of compound AJO14, we have designed and synthesized 21 AJO14 derivatives (named LZX-2-xx), aiming to improve its cytotoxic activity. In addition, other 30 AJO14-derived compounds were synthesized by EDELRIS (Lyon, France) as a custom service (named EDxx). Their code, structures, synthetic protocol, formula, molecular weight and characterization data are presented in Supplementary Table 1. The new designs focused on enhancing specific chemical moieties in the structures of these analogs. This enhancement included modifications such as substituting some of the hydrogens in the urea moiety, replacing or adding electron-withdrawing groups, and adjusting the positions of large substituents on the phenyl rings. Additionally, larger alkyl or aromatic groups were introduced to the sulfone moiety to potentially improve the IC_{50} values. Lastly, to enhance the metabolic stability of these compounds, the double bond in the cyclohexene ring of AJO14, and its initial analogs, was removed, and polar substituents were added.

Molecular docking

The binding of the compound LZX-2-73 to NUPR1 was investigated by using flexible docking at atomic detail, following a well-assessed protocol we had already used for in silico studies of the association of drugs to this IDP[17–19]. According to this protocol, the association of LZX-2-73 was simulated by modeling the conformation of a protein/ligand complex mimicking a transient binding pocket, in which the ligand was bound to a 5-residue fragment of the sequence of NUPR1 belonging to the hot spot region centered around the crucial residue Ala33. A second 5-residue fragment was also included in the subsequent simulation runs. Because of the large conformation heterogeneity and totally unstructured nature of NUPR1, which is preserved even when it is bound to any molecular partner, full flexibility was considered for both the ligand and the protein fragment

(or fragments). All the atoms in the molecular complex were explicitly considered, with the exception of apolar hydrogens subsumed to the carbon atom they are bound to. The modeling software AutoDock Tools, version 1.5.6[31] and the docking engine AutoDock Vina, version 1.2.3[45] were used to prepare the molecular system and perform the calculations, respectively. The simulations were performed by using the original AutoDock Vina scoring function[31], and Monte Carlo global optimization algorithm that includes a BFGS gradient-based optimizer. Default docking parameters were used in all cases, including for the exhaustiveness in the stochastic search. The compound LZX-2-73 was modeled by using the molecular editor Avogadro, version 1.2.0[46]. The 5-residue fragments of NUPR1 were capped with methyl groups, to avoid unwanted electrostatic effects due to the introduction of fictitious charged groups at both ends. For each fragment in extended conformation, the distance among the farthest atoms was < 25 Å; therefore, a search volume of 30 Å × 30 Å × 30 Å was sufficient to perform the docking simulations in all cases. At the end of the simulation procedure, the affinity was re-evaluated for the ten most favorable docking poses in which the ligand was sandwiched in between the two protein fragments, by using the MM-GBSA methodology as implemented in the fastDRH webserver[47]. The force fields Amber ff19SB[48] and GAFF2[49] were used for the protein and ligand, respectively, in combination with the OPC water model[50] Protein/ligand Interactions were not truncated (threshold radius ≥ 50 Å) beyond a cut-off.

Statistics

Statistical analyses were conducted by using one-way ANOVA, Dunnett's test or two-way ANOVA, Dunnett's test. The results were expressed as the mean ± SD of at least three independent experiments. A p-value < 0.05 was regarded as statistically significant.

Data availability

The datasets used and analyzed during the present study are available from the corresponding author on reasonable request.

References

1. Siegel, R. L., Miller, K. D., Wagle, N. S. & Jemal, A. Cancer statistics, 2023. *CA Cancer J. Clin.* **73**, 17–48 (2023).
2. Ilic, I. & Ilic, M. International patterns in incidence and mortality trends of pancreatic cancer in the last three decades: A joinpoint regression analysis. *World J. Gastroenterol.* **28**, 4698–4715 (2022).
3. Sung, H. et al. Global cancer statistics 2020: GLOBOCAN estimates of incidence and mortality worldwide for 36 cancers in 185 countries. *CA Cancer J. Clin.* **71**, 209–249 (2021).
4. Wang, S. et al. The molecular biology of pancreatic adenocarcinoma: Translational challenges and clinical perspectives. *Signal Transduct. Target Ther.* **6**, 249 (2021).
5. Werner, J. et al. Advanced-stage pancreatic cancer: Therapy options. *Nat. Rev. Clin. Oncol.* **10**, 323–333 (2013).
6. Vienot, A. et al. FOLFOXIRI vs FOLFIRINOX as first-line chemotherapy in patients with advanced pancreatic cancer: A population-based cohort study. *World J. Gastrointest. Oncol.* **12**, 332–346 (2020).
7. Riedl, J. M. et al. Gemcitabine/nab-paclitaxel versus FOLFIRINOX for palliative first-line treatment of advanced pancreatic cancer: A propensity score analysis. *Eur. J. Cancer* **151**, 3–13 (2021).
8. Cano, C. E., Hamidi, T., Sandi, M. J. & Iovanna, J. L. Nupr1: The swiss-knife of cancer. *J. Cell Physiol.* **226**, 1439–1443 (2011).
9. Goruppi, S. & Iovanna, J. L. Stress-inducible protein p8 is involved in several physiological and pathological processes. *J. Biol. Chem.* **285**, 1577–1581 (2010).
10. Santofimia-Castaño, P. et al. Targeting intrinsically disordered proteins involved in cancer. *Cell Mol. Life Sci.* **77**, 1695–1707 (2020).
11. Su, S. B. et al. Expression of p8 in human pancreatic cancer. *Clin. Cancer Res.* **7**, 309–313 (2001).
12. Sandi, M. J. et al. p8 expression controls pancreatic cancer cell migration, invasion, adhesion, and tumorigenesis. *J. Cell Physiol.* **226**, 3442–3451 (2011).
13. Cheng, Y. et al. Rational drug design via intrinsically disordered protein. *Trends Biotechnol.* **24**, 435–442 (2006).
14. Dunker, A. K. & Uversky, V. N. Drugs for 'protein clouds': Targeting intrinsically disordered transcription factors. *Curr. Opin. Pharmacol.* **10**, 782–788 (2010).
15. Uversky, V. N. Intrinsically disordered proteins and novel strategies for drug discovery. *Expert. Opin. Drug Discov.* **7**, 475–488 (2012).
16. Ruan, H., Sun, Q., Zhang, W., Liu, Y. & Lai, L. Targeting intrinsically disordered proteins at the edge of chaos. *Drug Discov. Today* **24**, 217–227 (2019).
17. Neira, J. L. et al. Identification of a drug targeting an intrinsically disordered protein involved in pancreatic adenocarcinoma. *Sci. Rep.* **7**, 39732 (2017).
18. Santofimia-Castaño, P. et al. Ligand-based design identifies a potent NUPR1 inhibitor exerting anticancer activity via necroptosis. *J. Clin. Invest.* **129**, 2500–2513 (2019).
19. Rizzuti, B. et al. Design of inhibitors of the intrinsically disordered protein NUPR1: Balance between drug affinity and target function. *Biomolecules* **11**, 1453 (2021).
20. Choi, S.-Y., Koh, Y.-S. & Jo, S.-H. Inhibition of human ether-a-go-go-related gene K+ channel and IKr of guinea pig cardiomyocytes by antipsychotic drug trifluoperazine. *J. Pharmacol. Exp. Ther.* **313**, 888–895 (2005).
21. Fermini, B. & Fossa, A. A. The impact of drug-induced QT interval prolongation on drug discovery and development. *Nat. Rev. Drug Discov.* **2**, 439–447 (2003).
22. Gintant, G., Sager, P. T. & Stockbridge, N. Evolution of strategies to improve preclinical cardiac safety testing. *Nat. Rev. Drug Discov.* **15**, 457–471 (2016).
23. Kalyaanamoorthy, S. & Barakat, K. H. Development of safe drugs: The hERG challenge. *Med. Res. Rev.* **38**, 525–555 (2018).
24. Garrido, A., Lepailleur, A., Mignani, S. M., Dallemagne, P. & Rochais, C. hERG toxicity assessment: Useful guidelines for drug design. *Eur. J. Med. Chem.* **195**, 112290 (2020).
25. Haverkamp, W. et al. The potential for QT prolongation and pro-arrhythmia by non-anti-arrhythmic drugs: Clinical and regulatory implications. Report on a policy conference of the European society of cardiology. *Cardiovasc. Res.* **47**, 219–233 (2000).
26. Lester, R. M., Paglialunga, S. & Johnson, I. A. QT Assessment in early drug development: The long and the short of it. *Int. J. Mol. Sci.* **20**, 1324 (2019).
27. Galluzzi, L., Kepp, O., Trojel-Hansen, C. & Kroemer, G. Mitochondrial control of cellular life, stress, and death. *Circ. Res.* **111**, 1198–1207 (2012).

28. Santofimia-Castaño, P. et al. NUPR1 protects against hyperPARylation-dependent cell death. *Commun. Biol.* **5**, 732 (2022).
29. Santofimia-Castaño, P. et al. Targeting the stress-induced protein NUPR1 to treat pancreatic adenocarcinoma. *Cells* **8**, 1453 (2019).
30. Santofimia-Castaño, P. et al. Amphipathic helical peptides hamper protein-protein interactions of the intrinsically disordered chromatin nuclear protein 1 (NUPR1). *Biochimica et Biophysica Acta BBA General Subjects* **1862**, 1283–1295 (2018).
31. Morris, G. M. et al. AutoDock4 and AutoDockTools4: Automated docking with selective receptor flexibility. *J. Comput. Chem.* **30**, 2785–2791 (2009).
32. Trott, O. & Olson, A. J. AutoDock Vina: Improving the speed and accuracy of docking with a new scoring function, efficient optimization, and multithreading. *J. Comput. Chem.* **31**, 455–461 (2010).
33. Rizzuti, B. Molecular simulations of proteins: From simplified physical interactions to complex biological phenomena. *Biochim. Biophys. Acta Proteins Proteom.* **1870**, 140757 (2022).
34. Mallo, G. V. et al. Cloning and expression of the rat p8 cDNA, a new gene activated in pancreas during the acute phase of pancreatitis, pancreatic development, and regeneration, and which promotes cellular growth. *J. Biol. Chem.* **272**, 32360–32369 (1997).
35. Wang, C. et al. SETD4 inhibits prostate cancer development by promoting H3K27me3-mediated NUPR1 transcriptional repression and cell cycle arrest. *Cancer Lett.* **579**, 216464 (2023).
36. Liu, J. et al. NUPR1 is a critical repressor of ferroptosis. *Nat. Commun.* **12**, 647 (2021).
37. Yammani, R. R. & Loeser, R. F. Brief report: Stress-inducible nuclear protein 1 regulates matrix metalloproteinase 13 expression in human articular chondrocytes. *Arthritis Rheumatol.* **66**, 1266–1271 (2014).
38. Encinar, J. A. et al. Human p8 is a HMG-I/Y-like protein with DNA binding activity enhanced by phosphorylation. *J. Biol. Chem.* **276**, 2742–2751 (2001).
39. Neira, J. L. et al. A phosphorylation-induced switch in the nuclear localization sequence of the intrinsically disordered NUPR1 hampers binding to importin. *Biomolecules* **10**, 1313 (2020).
40. Santofimia-Castaño, P. et al. Intrinsically disordered chromatin protein NUPR1 binds to the C-terminal region of Polycomb RING1B. *Proc. Natl. Acad. Sci.* **114**, E6332–E6341 (2017).
41. Bastos, M. et al. Isothermal titration calorimetry. *Nat. Rev. Methods Prim* **3** (2023).
42. Aguado-Llera, D. et al. Deciphering the binding between Nupr1 and MSL1 and their DNA-repairing activity. *PLoS One* **8**, e78101 (2013).
43. Santofimia-Castaño, P. et al. Inactivation of NUPR1 promotes cell death by coupling ER-stress responses with necrosis. *Sci. Rep.* **8**, 16999 (2018).
44. Nicolle, R. et al. A transcriptomic signature to predict adjuvant gemcitabine sensitivity in pancreatic adenocarcinoma. *Ann. Oncol.* **32**, 250–260 (2021).
45. Eberhardt, J., Santos-Martins, D., Tillack, A. F. & Forli, S. AutoDock Vina 1.2.0: New docking methods, expanded force field, and python bindings. *J. Chem. Inform. Model.* **61**, 3891–3898 (2021).
46. Hanwell, M. D. et al. Avogadro: an advanced semantic chemical editor, visualization, and analysis platform. *J. Cheminform.* **4**, 1–17 (2012).
47. Wang, Z. et al. fastDRH: A webserver to predict and analyze protein-ligand complexes based on molecular docking and MM/PB(GB)SA computation. *Brief Bioinform* **23**, bbac201 (2022).
48. Tian, C. et al. ff19SB: Amino-acid-specific protein backbone parameters trained against quantum mechanics energy surfaces in solution. *J. Chem. Theory Comput.* **16**, 528–552 (2020).
49. He, X., Man, V. H., Yang, W., Lee, T.-S. & Wang, J. A fast and high-quality charge model for the next generation general AMBER force field. *J. Chem. Phys.* **153**, 114502 (2020).
50. Izadi, S., Anandakrishnan, R. & Onufriev, A. V. Building water models: A different approach. *J. Phys. Chem. Lett.* **5**, 3863–3871 (2014).

Author contributions

X.L.: Resources, data curation, validation, investigation, methodology, writing-original draft; A.J-A.: Resources, data curation, validation, investigation and methodology; Z.L: Resources, data curation, validation, investigation and methodology; B.R.: Conceptualization, formal analysis, investigation; J.L. N.: Resources, data curation, validation, investigation and methodology; M.E.: Resources, data curation, validation, investigation and methodology; L.P.: Resources, data curation, validation, investigation and methodology; E.C.: Conceptualization, supervision, investigation; J.G.: Conceptualization, supervision, investigation; F.G.: Conceptualization, supervision, investigation; A.V-C.: Resources, data curation, validation, investigation, methodology, writing-review and editing; Y.X.: Resources, data curation, validation, investigation, methodology, writing-review and editing; O.A.: Resources, data curation, validation, investigation, methodology, writing-review and editing; P.S-C.: Conceptualization, data curation, formal analysis, supervision, funding acquisition, writing-original draft, project administration, writing-review and editing; J.I.: Conceptualization, data curation, formal analysis, supervision, funding acquisition, writing-original draft and editing, project administration.

Declarations

Competing interests
The authors declare no competing interests.

Ethical approval and consent to participate
All animal care and experimental procedures were performed in agreement with the Animal Ethics Committee of Marseille number 14 (C2EA-14). Approval Number: 202011181636926.

Additional information
Supplementary Information The online version contains supplementary material available at https://doi.org/10.1038/s41598-024-79340-z.

Correspondence and requests for materials should be addressed to P.S.-C. or J.I.

Reprints and permissions information is available at www.nature.com/reprints.

Publisher's note Springer Nature remains neutral with regard to jurisdictional claims in published maps and institutional affiliations.